

LETTER TO THE EDITOR

# An accurate measurement of the spectral resolution of the JWST Near Infrared Spectrograph

Anowar J. Shajib<sup>1,2,3</sup>, Tommaso Treu<sup>4</sup>, Alejandra Melo<sup>5,6</sup>, Guido Roberts-Borsani<sup>7</sup>, Shawn Knabel<sup>4</sup>, Michele Cappellari<sup>8</sup>, and Joshua A. Frieman<sup>1,2,9</sup>

- <sup>1</sup> Department of Astronomy & Astrophysics, University of Chicago, Chicago, IL 60637, USA; e-mail: ajshajib@uchicago.edu  
<sup>2</sup> Kavli Institute for Cosmological Physics, University of Chicago, Chicago, IL 60637, USA  
<sup>3</sup> Center for Astronomy, Space Science and Astrophysics, Independent University, Bangladesh, Dhaka 1229, Bangladesh  
<sup>4</sup> Department of Physics and Astronomy, University of California, Los Angeles, CA 90095, USA  
<sup>5</sup> Max Planck Institute for Astrophysics, Karl-Schwarzschild-Str. 1, Garching, 85748, Germany  
<sup>6</sup> Technical University of Munich, TUM School of Natural Sciences, Physics Department, James-Franck-Straße 1, 85748 Garching, Germany  
<sup>7</sup> Department of Physics & Astronomy, University College London, London, WC1E 6BT, UK  
<sup>8</sup> Sub-Department of Astrophysics, Department of Physics, University of Oxford, Denys Wilkinson Building, Keble Road, Oxford, OX1 3RH, UK  
<sup>9</sup> SLAC National Laboratory, 2575 Sand Hill Rd, Menlo Park, CA 94025

Received xxx, xxxx; accepted xxx, xxxx

## ABSTRACT

The spectral resolution ( $R \equiv \lambda/\Delta\lambda$ ) of spectroscopic data is crucial information for accurate kinematic measurements. In this letter, we present a robust measurement of the spectral resolution of the JWST’s Near Infrared Spectrograph (NIRSpec) in fixed slit (FS) and integral field spectroscopy (IFS) modes. Due to the similarity of the utilized slit dimension if the FS mode to that of the shutters in the multi-object spectroscopy (MOS) mode, our resolution measurements in the FS mode can also be used for the MOS mode in principle. We modeled H and He lines of the planetary nebula SMP LMC 58 using a Gaussian line spread function (LSF) to estimate the wavelength-dependent resolution for multiple disperser and filter combinations. We corrected for the intrinsic width of the planetary nebula’s H and He lines due to its expansion velocity by measuring it from a higher-resolution X-shooter spectrum. We find that NIRSpec’s in-flight spectral resolutions exceed the pre-launch estimates provided in the JWST User Documentation by 11–53% in the FS mode and by 1–24% in the IFS mode across the covered wavelengths. We recover the expected trend that the resolution increases with the wavelength within a configuration. The robust and accurate LSFs presented in this letter will enable high-accuracy kinematic measurements using NIRSpec for applications in cosmology and galaxy evolution.

**Key words.** Methods: observational – Techniques: spectroscopic – Methods: data analysis

## 1. Introduction

The JWST’s Near Infrared Spectrograph (NIRSpec; Böker et al. 2023) has enabled IR spectroscopy with an unprecedented combination of redshift reach, signal-to-noise ratio, and spatial resolution. One of its key applications is the study of stellar or gas kinematics in distant galaxies (e.g., de Graaff et al. 2024; Xu et al. 2024; Newman et al. 2025), helping us to understand their formation and evolution, the properties of gas outflows, and the impact of black hole and baryonic feedback (D’Eugenio et al. 2024). Furthermore, accurate measurement of the stellar velocity dispersion of lensing galaxies also enables high-precision measurement of the Hubble constant and other cosmological parameters through the method of time-delay cosmography (Shajib et al. 2025; TDCOSMO Collaboration 2025).

Accurate measurement of the line spread function (LSF) or the spectral resolution  $R \equiv \Delta\lambda/\lambda$ , where  $\Delta\lambda$  is the full width at half maximum (FWHM), is a prerequisite to robustly measuring the velocity dispersion  $\sigma_*$ . The LSF induces additional broadening in the observed lines, which can be parametrized with  $\sigma_{\text{inst}}$  assuming a Gaussian LSF. The accuracy requirement on  $\sigma_{\text{inst}}$  to achieve a desired level of accuracy on  $\sigma_*$  can be estimated using

the relation (Knabel et al. 2025)

$$\frac{\delta\sigma_*}{\sigma_*} \approx \frac{\delta\sigma_{\text{inst}}}{\sigma_{\text{inst}}} \left( \frac{\sigma_{\text{inst}}}{\sigma_*} \right)^2. \quad (1)$$

Therefore, achieving a 1% accuracy in the velocity dispersion, as desirable for precision cosmology (Knabel et al. 2025), requires an estimate of NIRSpec’s medium-resolution  $\sigma_{\text{inst}}$  accurate to 1.3% and 5.5% for  $\sigma_* = 150 \text{ km s}^{-1}$  and  $300 \text{ km s}^{-1}$ , respectively, for example.

NIRSpec’s LSF in the fixed-slit (FS) mode was previously measured from the narrow emission lines of the planetary nebula (PN) SMP LMC 58 (Isobe et al. 2023). These authors find that the resolution is higher by  $\sim 10\text{--}20\%$  than the pre-launch estimates provided by the JWST User Documentation (JDox).<sup>1</sup> These authors assumed that the intrinsic expansion velocity of the PN is negligible. However, if the true expansion velocity is near the upper limit of typical values (i.e.,  $\lesssim 30 \text{ km s}^{-1}$ ; Jacob et al. 2013), its impact may not be non-negligible, especially for the high-resolution grating ( $R \sim 2700$ ), which would

<sup>1</sup> JDox webpage for NIRSpec dispersers and filters

require a  $\sim 19\%$  correction ( $\sim 2.7\%$  for medium resolution with  $R \sim 1000$ ). Nidever et al. (2024) find the resolution in the multi-object spectroscopy (MOS) mode’s G140H/F100LP configuration to be  $\sim 50\text{--}85\%$  higher than the JDox estimates, using narrow absorption lines in red giant stars. Through modeling with simulated data in the MOS mode, de Graaff et al. (2024) attribute the discrepancy between direct measurements and JDox estimates to differences in the source morphology. These authors demonstrate that a point source would lead to  $\sim 50\text{--}90\%$  higher resolution in the MOS G395H/F290LP configuration than the JDox estimates, which are based on uniformly illuminated slits. However, the predicted resolution by de Graaff et al. (2024) did not account for the additional broadening introduced by the data reduction procedure. Hence, this value is not directly applicable to the reduced data, and a direct measurement from real data remains indispensable.

In this letter, we provide a wavelength-dependent parametrization of NIRSpec’s resolution for multiple disperser-filter combinations for all of its FS, integral field spectroscopy (IFS), and MOS modes. We measured the resolutions by fitting prominent H and He emission lines for the PN SMP LMC 58 using datasets from JWST calibration programs, which were specifically obtained for wavelength and LSF calibrations. Isobe et al. (2023) also used a subset of this dataset for their LSF measurements. The same PN was also targeted by Jones et al. (2023) to measure the LSF for JWST’s Mid-Infrared Instrument (MIRI). Most of the fitted H lines have nearby weaker He multiplets, which are partially or fully blended and need to be accounted for to obtain an accurate characterization of the LSF. As a significant improvement over previous studies, we account for all the blended lines. We simultaneously fit the medium- and high-resolution spectra, thereby allowing lines that are deblended in the high-resolution spectrum to inform their relative strengths when fitting the medium-resolution one. Furthermore, we corrected for the PN’s expansion velocity after directly measuring it from a higher-resolution ( $R \sim 6500$ ) spectrum of the same PN obtained using the Very Large Telescope’s (VLT) X-shooter instrument (Vernet et al. 2011).

This letter is organized as follows. In Section 2, we describe the JWST and X-shooter datasets we used. We describe our measurement method and provide the measured values in Section 3, and then conclude the letter in Section 4. Code scripts and notebooks used in this analysis are publicly available on GitHub.<sup>2</sup>

## 2. Datasets

We describe the NIRSpec dataset used to measure the spectral resolutions in Section 2.1 and the VLT X-Shooter spectra used to measure the PN’s expansion velocity in Section 2.2.

### 2.1. NIRSpec spectra

To provide instrument calibrations for the NIRSpec, the planetary nebula SMP LMC 58 (also known as IRAS 05248–7007) was observed with the calibration program CAL-1492 (PI: T. Beck). We utilized the FS and IFS mode spectra from this program.<sup>3</sup> The FS mode used the S200A1 slit with  $0\prime.2$  width, while

<sup>2</sup> [https://github.com/ajshajib/nirspec\\_resolution](https://github.com/ajshajib/nirspec_resolution)

<sup>3</sup> We do not utilize the MOS-mode observations from the program CAL-1492, as the exposures were stepped at 25 mas steps across the full pitch of an MSA shutter. Thus, the LSF in the stacked data is expected to have broadened beyond that from a point source centered on the slit with only sub-pixel dithers applied. However, due to the simi-

larity of the S200A1 slit dimension to the MSA shutters, the FS-mode values are theoretically expected to be a reasonable proxy for MOS-mode observations. Suitable MOS-mode datasets in the future can be easily analyzed with the code suite and notebooks we provided.

larity of the S200A1 slit dimension to the MSA shutters, the FS-mode values are theoretically expected to be a reasonable proxy for MOS-mode observations. Suitable MOS-mode datasets in the future can be easily analyzed with the code suite and notebooks we provided.

### 2.2. VLT X-shooter spectrum

The VLT X-shooter spectrum of the PN was obtained as part of an *Euclid*-preparation program (program ID 110.23Q7.001; *Euclid* Collaboration et al. 2023). The spectrum was obtained with the VIS arm (covering 550–1020 nm) using a  $1\prime.2$  slit, which has a nominal resolution of  $R \sim 6500$ .<sup>4</sup> We obtained the observed raw dataset from the European Southern Observatory (ESO) Science Portal,<sup>5</sup> along with the calibration files. We reduced the dataset to produce an extracted 1D spectrum using ESO’s X-shooter data reduction pipeline v3.8.1 (Modigliani et al. 2010) with ESOREFLEX v2.11.5.

## 3. Measurement of the NIRSpec resolution

We adopted the Gaussian profile to characterize the NIRSpec LSF. By testing on a single emission line ( $\text{Pa}\alpha$ ) that is not blended with other lines in both high and medium resolutions, we find that the LSF can be well-fitted with either a Gaussian or a Voigt profile, with the Voigt profile providing a better fit due to one additional degree of freedom. The Lorentzian profile, however, yields a significantly worse fit. We chose the Gaussian profile also because it is ubiquitously used to account for instrumental resolution in measurements of kinematics, for example, with the software program *pPXF* (Cappellari 2017, 2023). The resolution parameter  $R \equiv \lambda/\Delta\lambda$  relates to the associated instrumental dispersion  $\sigma_{\text{inst}}$  as  $R = c/(2.355\sigma_{\text{inst}})$ , where  $c$  is the speed of light. We parametrize the wavelength dependence of  $\sigma_{\text{inst}}(\lambda) = [\sigma'_{\text{inst}}(\lambda)^2 - \sigma_{\text{PN}}^2]^{1/2}$  as

$$\sigma_{\text{inst}}(\lambda) = \left[ \left\{ \frac{\sigma'_{\text{piv}}}{1 + \alpha(\lambda - \lambda_{\text{piv}}) / [1 \mu\text{m}]} \right\}^2 - \sigma_{\text{PN}}^2 \right]^{1/2}, \quad (2)$$

where  $\sigma'_{\text{inst}}(\lambda)$  is the instrumental dispersion not corrected for the PN’s expansion velocity  $\sigma_{\text{PN}}$ ,  $\sigma'_{\text{piv}}$  is the uncorrected instrumental dispersion at the pivot wavelength  $\lambda_{\text{piv}}$ , and  $\alpha$  is the coefficient in the inverse-linear dependence on wavelength. We chose the inverse-linear  $\lambda$ -dependence for  $\sigma'_{\text{inst}}$  because the resolution  $R \propto 1/\sigma_{\text{inst}}$  is found approximately linear in  $\lambda$  from the pre-launch estimates, given that  $\Delta\lambda$  tends to be approximately constant in wavelength units. We describe our measurement process for  $\sigma'_{\text{inst}}(\lambda)$  in Section 3.1 and for  $\sigma_{\text{PN}}$  in Section 3.2.

larity of the S200A1 slit dimension to the MSA shutters, the FS-mode values are theoretically expected to be a reasonable proxy for MOS-mode observations. Suitable MOS-mode datasets in the future can be easily analyzed with the code suite and notebooks we provided.

<sup>4</sup> <https://www.eso.org/sci/facilities/paranal/instruments/xshooter/inst.html>

<sup>5</sup> <https://archive.eso.org/scienceportal/>

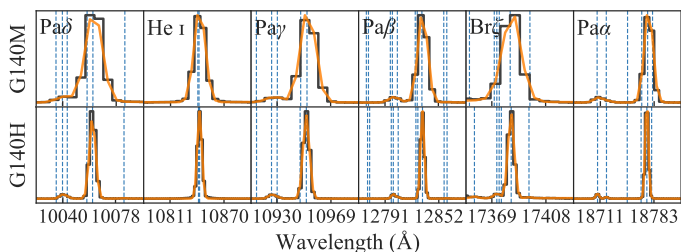


**Fig. 1.** Post-pixelized Gaussian profile fits (orange) to prominent emission-line groups (black) in the NIRSpec IFS spectra of the PN SMP LMC 58. The IFS-mode G140 disperser is illustrated here as an example among the nine combinations analyzed in this letter. The top row corresponds to the G140M/F100LP configuration (i.e., medium resolution), and the bottom row to G140H/F100LP (i.e., high resolution). The principal line within each group is annotated in the corresponding panel. The individual line wavelengths fitted in each group are marked with dashed blue lines. All of these lines are fitted simultaneously to directly constrain the parameters in  $\sigma'_{\text{inst}}(\lambda)$  from Eq. (2).

### 3.1. Emission line fitting from the NIRSpec spectra

We fit the spectra in wavelength slices around several prominent H and He emission lines. The details of the fitted wavelength ranges and the lists of lines within them are provided in Appendix A. Prominent H lines are often accompanied by He lines in proximity due to the resemblance in their atomic structures. Furthermore, He lines are usually multiplets. These lines are partially or fully blended, especially in the medium resolution. For a given combination of mode, disperser, and filter, we simultaneously fit all the lines within the chosen wavelength slices both in the high and medium resolution spectra, while individually constraining  $\sigma'_{\text{piv}}$  and  $\alpha$  for both gratings. The emission lines were fitted with post-pixelized (i.e., integrated within a pixel) Gaussian LSFs. The advantage of fitting all the lines together is that the information from all of them was aggregated to alleviate the issue that the LSF in most configurations is not critically sampled according to the Nyquist sampling theorem. The advantage of fitting both gratings together is that the relative line strengths could first be robustly constrained from the high-resolution spectrum, where they are less blended, which were then fixed for fitting the blended lines in the medium resolution (see Figure 1). We also fit for the PN's relative motion  $v_{\text{PN}}$  (previously measured as  $295 \pm 23 \text{ km s}^{-1}$ ; Reid & Parker 2006) without any dependency on the wavelength. We allowed the PN velocity to be independent between the medium- and high-resolution spectra to account for any residual offset in the wavelength calibration. In each wavelength slice, we fit the continuum level with a linear function. We additionally allowed a Gaussian intrinsic scatter  $\delta_{\text{intr}}$  in the  $\sigma_{\text{inst}}$  fitted to each line group around the mean relation of Eq. (2). Furthermore, we accounted for potential underestimation in the pipeline-produced uncertainties by allowing a systematic uncertainty floor  $\varepsilon_{\text{sys}}$  to vary freely for each resolution. Thus, we have 10 non-linear parameters characterizing the global properties of our generative model:  $\sigma'_{\text{piv}}$ ,  $\alpha$ ,  $v_{\text{PN}}$ ,  $\delta_{\text{intr}}$ , and  $\varepsilon_{\text{sys}}$  for each resolution. The amplitudes of the line profiles and the continuum levels were solved through linear inversion. We obtained the posteriors of the non-linear parameters (provided in Table 1) using the NAUTILUS sampler (Lange 2023).

**Table 1.** Best-fit values for parameters in the expression of  $\sigma'_{\text{inst}}(\lambda)$  in Eq. (2).

Disperser	Filter	$\lambda_{\text{piv}}$ (Å)	$\sigma'_{\text{piv}}$ (km s <sup>-1</sup> )	$\alpha$
<b>FS mode</b>				
G140M	F070LP	10111.02	$124.84 \pm 2.37$	$0.676 \pm 0.147$
G140H	F070LP	10111.02	$50.44 \pm 0.44$	$0.500 \pm 0.083$
G140M	F100LP	13347.24	$94.99 \pm 5.10$	$0.899 \pm 0.054$
G140H	F100LP	13347.24	$40.63 \pm 2.25$	$0.703 \pm 0.082$
G235M	F170LP	22765.89	$101.07 \pm 1.12$	$0.478 \pm 0.018$
G235H	F170LP	22765.89	$40.20 \pm 0.12$	$0.479 \pm 0.005$
G395M	F290LP	38474.54	$102.95 \pm 0.52$	$0.220 \pm 0.018$
G395H	F290LP	38474.54	$40.48 \pm 1.04$	$0.340 \pm 0.061$
<b>IFS mode</b>				
G140M	F100LP	13539.59	$117.01 \pm 2.25$	$0.668 \pm 0.035$
G140H	F100LP	13539.59	$46.36 \pm 1.05$	$0.699 \pm 0.036$
G235M	F170LP	22938.52	$112.74 \pm 0.59$	$0.488 \pm 0.008$
G235H	F170LP	22938.52	$42.75 \pm 0.28$	$0.398 \pm 0.010$
G395M	F290LP	38891.71	$105.74 \pm 0.56$	$0.251 \pm 0.014$
G395H	F290LP	38891.71	$41.98 \pm 0.70$	$0.239 \pm 0.026$

**Notes.** The value of  $\sigma_{\text{PN}}$  in Eq. (2) is measured in Section 3.2 to be  $\sigma_{\text{PN}} = 6.90 \pm 0.49 \text{ km s}^{-1}$ .

### 3.2. Measurement of the PN expansion velocity

To measure the expansion velocity of the PN from the X-shooter spectrum, we require a precise measurement of the spectral resolution of the X-shooter itself. We used the arc-lamp spectrum that was taken for wavelength calibration to obtain a wavelength-dependent estimate of X-shooter's spectral resolution. We used the PYPER software program (Prochaska et al. 2020) to measure the FWHMs of the arc-lamp lines in 15 wavelength bins within the covered wavelength range of 550–1020 nm (Figure 2). The uncertainty of the binned measurement was derived from the scatter in the individual-line measurements within each bin. The extent of the variation in the measured resolutions across the wavelength is qualitatively similar to that measured by Gonneau et al. (2020). We fit a quadratic function  $R_{\text{xsh}}(\lambda)$  to the measured points. We also simultaneously fit a post-pixelized Gaussian function to the H $\alpha$  line, which is the most prominent H line within the covered wavelengths. Although a few He lines also fall within the covered wavelength range, they do not significantly add to the constraining power due to their line strengths being smaller by 1.5 orders of magnitude or more. We parametrized the H $\alpha$  line's Gaussian profile with standard deviation  $[\sigma_{\text{PN}}^2 + c^2 / \{2.355R_{\text{xsh}}(\lambda_{\text{H}\alpha})\}^2]^{-1/2}$ , while allowing the peak position to vary to account for the PN's relative motion. We constrain the PN's expansion velocity  $\sigma_{\text{PN}} = 6.90 \pm 0.49 \text{ km s}^{-1}$ .

We illustrate the measured resolution curves for all the mode–disperser combinations in Figure 3 and compare them to the corresponding pre-launch estimates provided by JDox. The resolutions in the IFS mode across the covered wavelengths are higher by  $\sim 1$ –24% than the pre-launch estimates, whereas the resolutions in the FS mode are  $\sim 11$ –53% higher.

## 4. Conclusion

In this letter, we measured NIRSpec's spectral resolution in multiple configurations for in the FS and IFS modes. Due to the similarity in slit dimensions, the FS-mode resolution can be used as a reasonable proxy for the MOS mode. We provide a wavelength-dependent parametrization of the spectral resolution in terms of the instrumental dispersion  $\sigma_{\text{inst}}$  by fitting multiple H and He

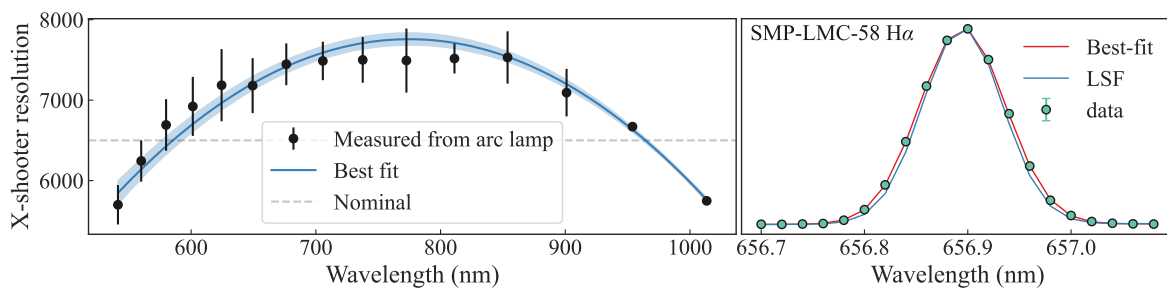


**Fig. 2.** Measurement of the PN's expansion velocity. *Left-hand panel:* Measurement of the X-shooter resolution (black points with error bars) from arc-lamp lines with the wavelength dependence modeled with a quadratic function (blue line, with the shaded region showing  $1\sigma$  uncertainty). *Right-hand panel:* The  $H\alpha$  line of the PN in the X-shooter spectra (emerald points). The error bars are too small to be noticeable here. The best-fit post-pixelized Gaussian profile is shown in red, while the width of the X-shooter LSF, as determined by the best fit in the left-hand panel, is shown in blue for comparison. Both sets of illustrated datapoints are simultaneously fit to infer the PN's expansion velocity  $\sigma_{\text{PN}} = 6.90 \pm 0.49 \text{ km s}^{-1}$ .

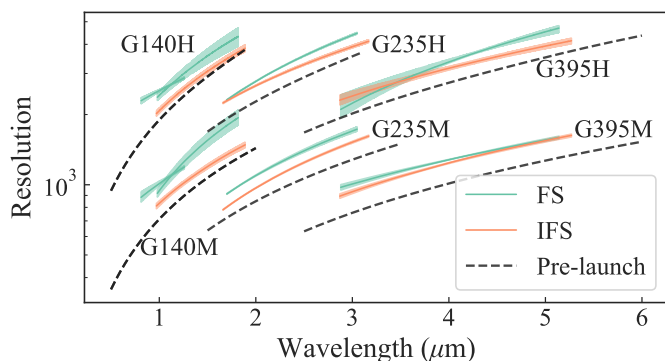


**Fig. 3.** Comparison of our measured resolution curves in the FS (emerald) and IFS (orange) modes with the pre-launch estimates from JDox (dashed grey lines). The shaded region around each resolution curve signifies the  $1\sigma$  credible region. The in-flight resolutions are 11–53% higher than the pre-launch estimates in the FS mode, and 1–24% higher in the IFS mode (across the covered wavelengths).

emission lines across the observed wavelength range in the PN SMP LMC 58. We incorporated a correction for the intrinsic width of the PN's lines, which we measured using a higher-resolution X-shooter spectrum of the same PN. Our measured resolutions are directly applicable for point source spectra; however, caution is advised when using them for extended sources.

The measured resolutions increase with wavelength in all configurations, as expected from the pre-launch estimates provided by JDox. For the FS mode, our measured resolution values extend up to 20% higher than those found by [Isobe et al. \(2023\)](#), potentially due to our methodology allowing multiple lines to be fitted within a blended line group. Our measured resolution in the G140H/F100LP configuration is smaller than that found by [Nidever et al. \(2024\)](#), which may be a difference between single-exposure and stacked spectra. Therefore, caution is advised when applying our measured value for datasets with drastically different dithering procedures from CAL-1492.

The parametric wavelength-dependent functions we provide will enable accurate measurements of kinematics from the NIR-Spec data, as performed, e.g., by [TDCOSMO Collaboration \(2025\)](#) and [Shajib et al. \(2025\)](#). Although we do not provide the MOS-mode values at the medium resolution, the FS-mode values in medium resolution can be used as a substitute following [Isobe et al. \(2023\)](#), as the slit width for the analyzed data in the FS mode is the same as that of the multi-shutter-array slitlets.

**Acknowledgements.** We thank David Nidever for helpful comments as the referee, which improved this manuscript. We thank Hsiao-Wen Chen, Danial Rangavar Langeroodi, Mark Morris, and Stefan Noll for useful discussions. This work is based on observations made with the NASA/ESA/CSA James Webb Space Telescope. The data were obtained from the Mikulski Archive for Space Telescopes at the Space Telescope Science Institute, which is operated by the Association of Universities for Research in Astronomy, Inc., under NASA contract NAS 5-03127 for JWST. These observations are associated with programs #1125 and 1492. The specific observations analyzed can be accessed via <https://dx.doi.org/10.17909/m3c0-3t58>. AJS and TT acknowledge support from NASA through STScI grants JWST-GO-2974, HST-GO-16773, and JWST-GO-1794. This research made use of NUMPY ([Oliphant 2015](#)), SCIPY ([Jones et al. 2001](#)), ASTROPY ([Astropy Collaboration 2013, 2018](#)), JUPYTER ([Kluyver et al. 2016](#)), MATPLOTLIB ([Hunter 2007](#)), SEABORN ([Waskom et al. 2014](#)), and NAUTILUS ([Lange 2023](#)).

## References

- Astropy Collaboration. 2013, *A&A*, 558, A33  
 Astropy Collaboration. 2018, *AJ*, 156, 123  
 Böker, T., Beck, T. L., Birkmann, S. M., et al. 2023, *Publications of the Astronomical Society of the Pacific*, 135, 038001  
 Bushouse, H., Eisenhamer, J., Dencheva, N., et al. 2023, *JWST Calibration Pipeline*  
 Cappellari, M. 2017, *MNRAS*, 466, 798  
 Cappellari, M. 2023, *MNRAS*, 526, 3273  
 de Graaff, A., Rix, H.-W., Carniani, S., et al. 2024, *A&A*, 684, A87  
 D'Eugenio, F., Pérez-González, P. G., Maiolino, R., et al. 2024, *Nature Astronomy*, 8, 1443  
 Euclid Collaboration, Paterson, K., Schirmer, M., et al. 2023, *A&A*, 674, A172  
 Gonneau, A., Lyubenova, M., Lançon, A., et al. 2020, *A&A*, 634, A133  
 Hunter, J. D. 2007, *Computing in Science and Engineering*, 9, 90  
 Isobe, Y., Ouchi, M., Nakajima, K., et al. 2023, *ApJ*, 956, 139  
 Jacob, R., Schönberner, D., & Steffen, M. 2013, *A&A*, 558, A78  
 Jones, E., Oliphant, T., Peterson, P., & Others. 2001, *SciPy: Open Source Scientific Tools for Python*  
 Jones, O. C., Alvarez-Márquez, J., Sloan, G. C., et al. 2023, *MNRAS*, 523, 2519  
 Kluyver, T., Ragan-Kelley, B., Pérez, F., et al. 2016, in *Positioning and Power in Academic Publishing: Players, Agents and Agendas*, ed. F. Loizides & B. Schmidt (IOS Press BV, Amsterdam, Netherlands), 87–90  
 Knabel, S., Mozumdar, P., Shajib, A. J., et al. 2025, *TDCOSMO XIX: Measuring Stellar Velocity Dispersion with Sub-Percent Accuracy for Cosmography*  
 Lange, J. U. 2023, *MNRAS*, 525, 3181  
 Modigliani, A., Goldoni, P., Royer, F., et al. 2010, in *Observatory Operations: Strategies, Processes, and Systems III*. Vol. 7737, 773728  
 Newman, A. B., Gu, M., Belli, S., et al. 2025, *arXiv e-prints*, arXiv:2503.17478  
 Nidever, D. L., Gilbert, K., Tollerud, E., et al. 2024, in *IAU Symposium*, Vol. 377, *Early Disk-Galaxy Formation from JWST to the Milky Way*, ed. F. Tabatabaei, B. Barbuy, & Y.-S. Ting, 115–122  
 Oliphant, T. E. 2015, *Guide to NumPy*, 2nd edn. (USA: CreateSpace Independent Publishing Platform)  
 Prochaska, J., Hennawi, J., Westfall, K., et al. 2020, *JOSS*, 5, 2308  
 Reid, W. A. & Parker, Q. A. 2006, *Monthly Notices of the Royal Astronomical Society*, 373, 521  
 Shajib, A. J., Treu, T., Suyu, S. H., et al. 2025, *arXiv e-prints*, arXiv:2506.21665  
 TDCOSMO Collaboration. 2025, *arXiv e-prints*, arXiv:2506.03023  
 van Hoof, P. A. M. 2018, *Galaxies*, 6, 63  
 Vernet, J., Dekker, H., D'Odorico, S., et al. 2011, *A&A*, 536, A105  
 Waskom, M., Botvinnik, O., Hobson, P., et al. 2014, *Seaborn: V0.5.0* (November 2014)  
 Xu, Y., Ouchi, M., Yajima, H., et al. 2024, *ApJ*, 976, 142

## Appendix A: Fitted line lists

In this appendix, we provide the list of fitted lines within the chosen wavelength ranges in Tables A.1, A.2, and A.3 for the G140, G235, and G395 dispersers, respectively. We first obtained a comprehensive list of nebular H and He lines from the Atomic Line List database<sup>6</sup> (van Hoof 2018). We then aggregated He lines that are close to each other within 1/8th of a pixel size in the corresponding high-resolution spectrum into a single line with an average wavelength weighted by the transition probability (i.e., the Einstein coefficient  $g_k A_{ki}$ ). We adopted 1/8 of the pixel size here, as this is half of the target threshold for wavelength calibration error (Böker et al. 2023). Thus, lines that are separated more closely can be sufficiently considered indistinguishable in the spectrum. Not all the line groups were fitted in some modes, as those line groups fall fully or partially outside of the covered wavelength range in the particular modes. The tables in this appendix specify the modes for which each line group was fitted.

**Table A.1.** Line list in the fitted wavelength ranges for the G140 disperser.

Principal Line	$\lambda_{\min}$ (Å)	$\lambda_{\max}$ (Å)	H lines (Å)	He lines (Å)	Mode
Pa $\eta$	8980	9060	9017.385	8999.448, 9002.207, 9011.625, 9013.688	FS (070LP)
Pa $\zeta$	9190	9290	9231.547	9212.861, 9215.757, 9227.763, 9230.392	FS (070LP)
Pa $\delta$	10020	10100	10052.128	10025.946, 10030.471, 10033.901 10048.008, 10074.794	FS (F100LP), IFS
He	10780	10900	–	10832.057, 10833.273	FS (F100LP), IFS
Pa $\gamma$	10910	10990	10941.090	10905.195, 10915.994, 10920.055 10936.607	FS, IFS
Pa $\beta$	12760	12885	12821.590	12759.178, 12761.554, 12786.127 12788.433, 12794.005, 12814.100 12816.340, 12846.135, 12849.524	FS (F100LP), IFS
Br $\zeta$	17350	17430	17366.850	17340.346, 17356.484, 17358.152 17359.750, 17379.672	FS (F100LP), IFS
Pa $\alpha$	18675	18820	18756.130	18690.446, 18702.347, 18730.012 18748.470, 18762.520	IFS

**Notes.** The  $\lambda_{\min}$  and  $\lambda_{\max}$  columns provide the limits of the fitted wavelength ranges. The mode column provides the modes for which the corresponding line group was included in the fit.

<sup>6</sup> v.300b5: <https://linelist.pa.uky.edu/newpage/>

**Table A.2.** Line list in the fitted wavelength ranges for the G235 disperser.

Principal Line	$\lambda_{\min}$ (Å)	$\lambda_{\max}$ (Å)	H lines (Å)	He lines (Å)	Mode
Br $\eta$	16800	16850	16811.111	16801.166, 16802.417, 16804.238 16812.264	IFS
Br $\zeta$	17300	17440	17366.850	17332.122, 17334.426, 17340.346 17356.484, 17358.152, 17359.750 17379.672	FS, IFS
Pa $\alpha$	18655	18840	18756.130	18690.446, 18702.347, 18730.012 18748.470, 18762.520	FS, IFS
He	20555	20660	–	20565.536, 20582.065, 20586.905 20592.793, 20605.478, 20607.440 20622.819	FS, IFS
Br $\gamma$	21575	21750	21661.200	21586.002, 21613.713, 21622.911 21633.577, 21647.434, 21652.342 21655.380	FS, IFS
Br $\beta$	26180	26350	26258.670	26192.126, 26205.629, 26240.932 26247.940, 26254.427, 26259.100	FS, IFS
Pf $\eta$	30350	30480	30392.022	30337.982, 30348.429, 30357.263 30373.932, 30378.344, 30379.607 30399.159, 30408.587	IFS

**Notes.** The  $\lambda_{\min}$  and  $\lambda_{\max}$  columns provide the limits of the fitted wavelength ranges. The mode column provides the modes for which the corresponding line group was included in the fit.

**Table A.3.** Line list in the fitted wavelength ranges for the G395 disperser.

Principal Line	$\lambda_{\min}$ (Å)	$\lambda_{\max}$ (Å)	H lines (Å)	He lines (Å)	Mode
Pf $\eta$	30330	30520	30392.022	30318.738, 30323.249, 30337.982 30348.429, 30357.263, 30373.932 30378.344, 30379.607, 30399.159 30408.587, 30444.836, 30476.839	FS, IFS
Pf $\gamma$	37350	37580	37405.560 37493.933	37328.390, 37344.208, 37381.965 37388.446, 37390.291, 37393.705 37397.995, 37411.662, 37440.355 37442.284, 37450.136, 37473.193 37474.795, 37477.586, 37478.614 37483.145	FS, IFS
Br $\alpha$	40300	40730	40522.620	40377.329, 40391.224, 40409.405 40490.196, 40506.090, 40512.200 40544.911, 40563.509, 40574.568	FS, IFS
He	42900	43100	–	42954.167, 42959.415	FS, IFS
Hu $\zeta$	43725	43900	43764.544	43708.509, 43739.438, 43744.948 43746.575	FS, IFS
Hu $\delta$	51230	51450	51286.570	51195.942, 51212.387, 51214.216 51216.767, 51255.944, 51263.452 51265.485, 51267.336, 51271.545 51273.953, 51341.610	IFS

**Notes.** The  $\lambda_{\min}$  and  $\lambda_{\max}$  columns provide the limits of the fitted wavelength ranges. The mode column provides the modes for which the corresponding line group was included in the fit.